*Int. J. Heat Mass Transfer.* Vol. 8, pp. 1153–1169. Pergamon Press 1965. Printed in Great Britain

# THE EFFECT OF GAS FLOW PATTERNS ON RADIATIVE TRANSFER IN CYLINDRICAL FURNACES

H. C. HOTTEL and A. F. SAROFIM
Department of Chemical Engineering, Massachusetts Institute of Technology

(*Received* 4 *December* 1964 *and in revised form* 1 *March* 1965)

**Abstract**—The prediction of performance of industrial furnaces is conventionally estimated by making gross assumptions as to the effect of temperature variations in the gas. The zone method of allowing for the effect, on radiative transfer, of the temperature variation in furnace enclosures has been applied to the problem of interaction between radiation and other modes of heat transfer. The effect of different flow patterns on the gas temperature-field and wall-flux distribution in a cylindrical furnace has been examined by use of the following flow models: plug flow; parabolic velocity profiles; ducted-jet flow (axial feed) with recirculation rates of 0, 1, and 11 times the flue-gas flow rate. A sixteenfold range of diameters and firing densities was studied. The reduced efficiencies were correlated, for a fixed surface temperature and for each of the flow models, in terms of a reduced firing rate. The wide range of heat flux distribution patterns found in the study emphasizes the need to include allowance for gas temperature variation in any furnace analysis in which the heat flux pattern is important.

## NOMENCLATURE

$a(\,)$, $a'(\,)$, weighting for calculating absorptivity (emissivity) of gases, dimensionless. $n^{\text{th}}$ term in series $a_n(\,)$, term in parenthesis temperature of emitter;

$A$, area of surface zone;

$B$, characteristic length of a zone;

$Ct$, Craya–Curtet number, see Appendix A;

$D'$ reduced firing density, equation (14).

$E$, blackbody emissive power, $= \sigma T^4$ [energy/time area];

$\overline{gg}$, $(\overline{gs})$, direct-exchange area for interchange between two gas zones (between a gas and a surface zone);

$\overline{GG}$, $(\overline{GS})$, total-interchange area between two gas zones (between a gas and surface zone);

$(\overline{GG})_n$, $(\overline{GS})_n$, total-interchange areas evaluated for $K = K_n$;

$\vec{GG}$, $\vec{GS}$, directed-flux areas, the $a$-weighted sum of total exchange areas. Parenthesis and a subscript $R$ indicates allowance for adiabatic refractory surface in evaluation of directed-flux areas;

$h$, convective heat-transfer coefficient;

$\dot{H}_{\text{in}}$ enthalpy of fuel and air streams entering the furnace per hour measured above a base temperature of absolute zero and the dead state $CO_2$, $H_2O(v)$, $O_2$, $N_2$;

$i_N$, $(i_I)$, momentum flux of nozzle fluid (of induced air stream);

$K$, absorption coefficient, reciprocal length;

$L$, path length;

$\dot{m}_N$, $(\dot{m}_I)$, mass flux of nozzle fluid (of induced air stream);

$\dot{M}C_p$, average hourly heat capacity of combustion products over the temperature range 0 to $T_g$;

$Nu$, Nusselt number;

$Pr$, Prandtl number;

$\dot{Q}$, energy flux rate;

$\dot{Q}_R$, reduced energy flux rate, $\dot{Q}/\dot{H}_{\text{in}}$;

| | |
|---|---|
| $Re$, | Reynolds number; |
| $ss$, | surface-to-surface direct-exchange area; |
| $\overline{SS}$, $(\overline{\hat{S}\hat{S}})$, | surface-to-surface total exchange area (directed-flux area); |
| $T$, | absolute temperature; |
| $u_d$, | dynamic-mean velocity, equation (A-2); |
| $u_k$, | kinematic-mean velocity, equation (A-1); |
| $V$, | volume of gas zone; |
| $\alpha_{gs}$, | gas absorptivity; |
| $\epsilon_g$, $(\epsilon_w, \epsilon_e)$, | emissivity of gas (surface); |
| $\rho$, | gas density; |
| $\sigma$, | Stefan–Boltzmann constant; |
| $\tau$, | reduced surface temperature, $T_w/T_{AF}$. |

Subscripts

| | |
|---|---|
| $e$, | end wall; |
| $g$, | gas; |
| $w$, | circumferential wall. |

THE EFFICIENCY and heat-transfer distribution in furnace combustion chambers involve such a complicated interaction among the energy terms associated with radiation, convection, conduction, and combustion that a rigorous analysis is out of the question. Early calculations of furnace performance were based on one of two models: a well-stirred furnace in which the radiating gases could be assigned a single mean temperature [10]; and a furnace in which the dimension in the direction of flow is so long compared to the other two that the flux to the walls at any distance from one end can be evaluated in terms of only the local conditions [10]. Growing concern with high temperature processes and especially with the details of the heat flux distribution within processing furnaces has emphasized the need for an evaluation of the effect of temperature gradients within the furnace. A rigorous treatment must depend on knowledge of flow patterns, patterns of combustion progress, a description of gas absorbing and emitting characteristics, and a method of allowing for the effect of the complex geometry of a furnace on the radiative interchange among all its parts. Sufficient progress has been made in these areas recently to justify attempting a synthesis of their effects to determine the complete temperature field of the furnace volume and walls and the resultant pattern of heat-flux distribution.

In this paper a partial idealization of a furnace that retains the most important features of a real system will be used to show, in a nearly rigorous way, the effect of flow patterns on efficiency and wall heat-flux distribution in cylindrical furnaces. The extensive recent publications on radiation from non-isothermal gases usually treat highly idealized systems; they have been adequately reviewed elsewhere [15, 20] and will not be considered in this paper.

## SYSTEM DESCRIPTION

### *Furnace configuration*

A right circular cylindrical furnace was selected for study in order to take advantage of the symmetry, the availability of radiative exchange factors [7] and the recent definition of the flow field for this configuration. A furnace length-to-diameter ration of 8/3 and diameters of 1, 4, and 16 ft were selected for study. The circumferential wall was treated as a gray heat sink at a temperature of 1460°R and emissivity 0·8, the end walls as adiabatic (refractory) surfaces of emissivity 0·5. The end walls can be considered to be baffled refractories inasmuch as they present a uniform surface to incident radiation and yet allow free passage of gas. This somewhat artificial completion of the enclosure eliminates the need for considering radiative interaction of the enclosure with the flue-gas exit system.

### *Fuel and air preheat*

It was postulated that the furnace was fired with a fuel $(CH_2)_x$ having a net heat of combustion of 19150 Btu/lb; and that the entering air, 15 per cent in excess of that required for stoichiometric combustion, was preheated to 1460°R. The adiabatic flame temperature for the conditions selected is 4525°R (no use is made of this quantity).

### *Flow patterns*

Five flow patterns were selected: plug flow; a parabolic self-repeating velocity profile; and

three patterns approximating those formed by a turbulent jet axially fired into a uniform air stream. The flow patterns of a ducted-jet system have been shown to depend on a dimensionless parameter known as the Craya–Curtet number ($Ct$), in turn dependent on the mass and momentum ratios of the jet flow to the induced flow ([1, 4]; and see Appendix A). $Ct$'s near zero correspond to high-momentum jets and high ratios of recirculation to total net flow; recirculation stops when $Ct$ exceeds 0·74. The three ducted-jet flow patterns studied here correspond to Craya–Curtet numbers of 0·51, 0·18, and 0·033, or to recirculatory flow rates 0·075, 1·44, and 10·91 times the flue-gas flow rate. The effect of temperature gradients, combustion, and energy transfer on the flow patterns was neglected. Although this simplification might at first appear to introduce excessive error, convincing evidence exists of the ability to model flame structures with cold-flow systems [3]. Figure 1 shows approximate positions of the mean-stream lines (lines across which the time-average mass flux is zero) for the three jet-flow patterns. The recirculation ratio is identifiable with the ratio of the number of mean-stream

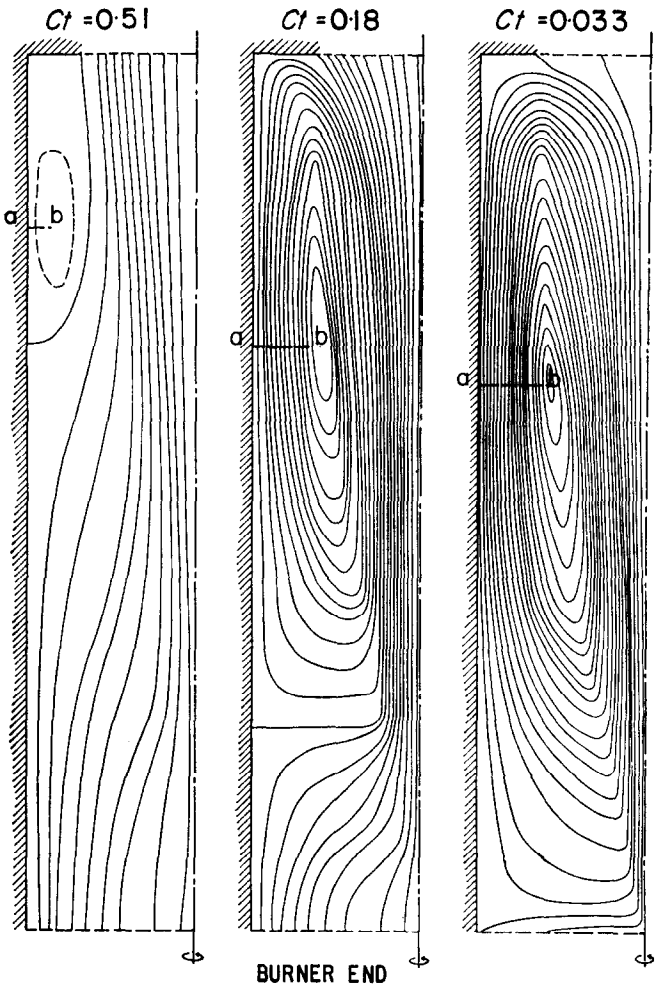


FIG. 1. Mean flow patterns for a cylindrical furnace fired axially (flow between mean streamlines for $Ct = 0{\cdot}033$ is five times the value at $Ct$'s of 0·18 and 0·51). Because of symmetry, the patterns to the left of the axis only are shown.

tubes in reverse flow along line ab—extending from the "eye" of the recirculation eddy to the wall—to the number crossing the entrance boundary at the bottom. Although the flow pattern based on a duct of unlimited length indicates the existence of recirculation from beyond the end of the present furnace, this was ignored; flue gas was assumed to flow out through the central end area occupying two-thirds of the furnace diameter.

*Combustion patterns*

For the uniform and parabolic velocity profiles the combustion was assumed to be completed within the row of gas zones adjacent to the feed-end wall, with the energy release rate distributed radially in the same proportion as the gas flow rate. For the axially fired jet the progress of combustion depends on the rate and intimacy of mixing of fuel and air, and can be estimated, for any point in the furnace, from the time-mean value of the fuel concentration and the amplitude of its fluctuation [9]. The patterns of mean value and amplitude were obtained from Becker's cold-flow study of mixing in ducted jets [2]. For $Ct$'s of 0·51 and 0·18, 6 and 16 per cent of the total air was arbitrarily assumed to be premixed with the fuel in the primary jet. When the furnace is subdivided into 8 axial sections, each with 3 radial subdivisions (Fig. 2) the above treatment of combustion indicates that for the three values of the Craya–Curtet number selected, all combustion occurs in the central radial zone and is distributed along the axis in the patterns given in Table 1.

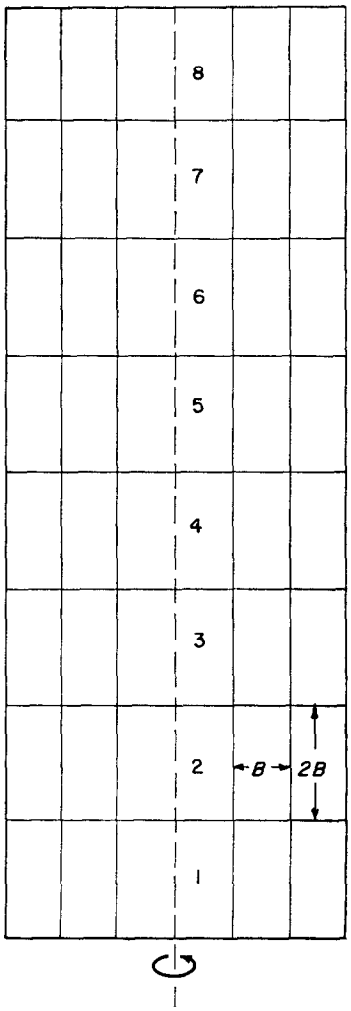


FIG. 2. Cross-section through furnace, showing subdivision into zones.

*Convection and eddy diffusion coefficients*

An estimate of the convective heat-transfer coefficient $h$ at the circumferential walls was obtained by assuming that

$$Nu = 0{\cdot}23\, Pr^{0{\cdot}4}\, Re^{0{\cdot}8} \qquad (1)$$

The Reynolds and Nusselt numbers were evaluated using the velocity at the wall external to the jet plume, as calculated from Becker's results, and a characteristic dimension of 4 in.

*Table 1. Per cent of fuel burned in the different zones along the axis*

| Craya–Curtet number | Zone number 1 | 2 | 3 | 4 | 5 | 6 | 7 | 8 |
|---|---|---|---|---|---|---|---|---|
| 0·51 | 18·5 | 17 | 16 | 13 | 10·5 | 10 | 8 | 7 |
| 0·18 | 45 | 17 | 11 | 10 | 10 | 7 | 0 | 0 |
| 0·033 | 100 | 0 | 0 | 0 | 0 | 0 | 0 | 0 |

such as might be found in a row of refractory-backed tubes. The coefficients to the end walls were estimated from values reported for flow normal to a plate [8]. Based on the further assumption that $h$ had a minimum value of 1·5 Btu/h ft² degF, the values of Table D1 in the Appendix were obtained. These coefficients are very approximate; fortunately errors in the convection coefficient introduce little error in the calculated fluxes to the walls since the radiative flux is usually dominant. The eddy diffusion coefficients at the boundaries of the gas zones were evaluated from Becker's values of the correlation coefficients of concentration fluctuations, the velocity field, and the concentration field in a ducted turbulent jet. Other design or operational variables are included in the summary Table 2.

## CALCULATION PROCEDURE

The method used to calculate the gas-temperature distribution and the wall-heat flux distribution is described in earlier papers [11, 14]. The major steps in the calculation will now be presented without derivation:

(a) *description of gas emissivity and absorptivity*

The problem is restricted to non-luminous radiation from the combustion products of the $CH_2)_x$ fuel, i.e. an equimolal mixture of $CO_2$ and $H_2O$ each with a partial pressure of 0·115 atm. The emissivity $\epsilon$ and absorptivity $\alpha$ as a function of temperature and path length are evaluated using the emissivity charts for $CO_2$ and $H_2O$ in [10] and a new correction chart for the overlap of the 2·7 $\mu$ and 15 $\mu$ bands [18]. The resulting values are described, for a range of temperature $T$ and path length $L$ of interest, by the following series which may be visualized as representing the gas as a mixture of "gray" gases:

$$\epsilon_g = [a_1'(T_g)]\,[1 - \exp(-K_1 L)] + [a_2'(T_g)]\,[1 - \exp(-K_2 L)] + [a_3'(T_g)]\,[1 - \exp(-K_3 L)] \quad (2)$$

$$\alpha_{g,\,s} = [a_1(T_s)]\,[1 - \exp(-K_1 L)] + [a_2(T_s)]\,[1 - \exp(-K_2 L)] + [a_3(T_s)]\,[1 - \exp(-K_3 L)] \quad (3)$$

where $a(T)$ indicates that the weighting factor $a$ is a function of $T$. The advantage of the above description is that it accurately describes the experimental emissivities over a 200-fold path length range, that by use of temperature-dependent $a$-weighting factors allowance is made for the major effect of temperature on the spectral energy distribution of the emitter, be it surface or gas, and that multiple-reflection effects in the radiative exchange may be treated in the same way as for gray gases. The values of $a$ and $K$ are tabulated in the Appendix. The complements of the sums of the $a$-weighting factors;

$$a_0 = 1 - a_1 - a_2 - a_3$$

and

$$a_0' = 1 - a_1' - a_2' - a_3'$$

represent the fraction of the energy spectrum in which $K = 0$, i.e. the "windows" of the spectrum through which surfaces freely exchange radiation.

*Table 2. Summary of design and operational variables*

| | |
|---|---|
| Length to diameter ratio | 8/3 |
| Diameter | 1, 4, and 16 ft |
| Emissivity of sink (The entire circumferential wall) | 0·8 |
| Emissivity of refractory (both end walls) | 0·5 |
| Sink temperature | 1460°R |
| Fuel | $(CH_2)_x$, $-\Delta H = 19\,150$ Btu/lb |
| Excess air | 15% |
| Air preheat | 1460°R |
| Firing rates | 9850; 39 400; and 157 600 Btu/h ft² of sink area* |
| Flow and combustion patterns | $Ct$ 0·51, 0·18, 0·033; Plug-flow and parabolic velocity profiles with rapid combustion |

* These values are the enthalpy of the fuel and air above a base of 520°R. The three firing rates will hereafter be referred to by the nominal values of $10^4$, $4 \times 10^4$, and $16 \times 10^4$ Btu/h ft².

(b) *Zoning of the enclosure*

The enclosure is divided into eight sections along the axis, each of length 2B; and each section is divided into three coaxial cylinder rings in such a way that the radius of the innermost cylinder shell and the distance between one cylinder shell and the next are B (Fig. 2). This subdivision gives 24 gas zones, 8 cylindrical sink zones, and 6 adiabatic refractory zones. The adequacy of the subdivision will be discussed later.

(c) *Direct-exchange areas*

It may readily be shown that the direct interchange between two finite zones, gray gas and/or black surface, of any shape and relative disposition and with gray absorbing gas intervening, is proportional to the difference in black emissive power $E(\equiv \sigma T^4)$ of the zones; and the proportionality constant, which must have the dimensions of area, is a function only of the system shape and of $KL$ where $L$ is a characteristic dimension of the system. The proportionality constant, designated by $\overline{ss}$, $\overline{sg}$, or $\overline{gg}$, is called the direct-exchange area [11]. The direct-exchange areas between all zone pairs in the enclosure, for $KB$'s corresponding to each of the 3 values of $K$ in equations (2) and (3), are determined from tabulations given by Erkku [7]. No allowance is made for any variation in gas composition; it is assumed everywhere to be that of the leaving flue gas. Exchange areas between surface zone pairs are also evaluated for the clear-gas component ($K = 0$) in the gas.

(d) *Total-exchange areas*

Radiation from a zone may reach a second both directly and after one or more reflections at the bounding surfaces. Allowance for the multiply reflected beams can be made by the methods of [11]. For a gray gas the total flux between two zones $i$ and $j$ must be proportional to $\sigma(T_i^4 - T_j^4)$; and the proportionality constant, called the total exchange area, is indicated by capital letters $\overline{SS}$, $\overline{GS}$, or $\overline{GG}$ ($S$ = surface, $G$ = gas), with subscripts to identify zone number. The total-exchange areas between all zone pairs are evaluated from direct-exchange areas for each gray-gas component, i.e. for each value of $K$. When $KB$ for a zone is greater than 0·4, it is no longer permissible to neglect temperature gradients within a gas zone. For such cases the direct-exchange area may be modified by the approximate techniques given in [14]; for values of $KB$ exceeding three, the total-exchange areas between contiguous zone pairs are calculated using the Rosseland diffusion equation [17].

(e) *The directed-flux areas*

The temperature field is estimated and the $a$-weighting factors for emissivity and absorptivity are evaluated for all surface and gas zones. This enables the evaluation of the radiative exchange between all zone pairs. For example, the radiative exchange between a surface zone $i$ of black emissive power $E_{s,i}$ and a gas zone $j$ of black emissive power $E_{g,j}$ is given by

$$\begin{aligned} \dot{Q}_{A_i \rightleftharpoons V_j} &= \{\sum_{n=1}^{3} [a_n(T_i)] (\overline{S_iG_j})_n\} E_{s,i} \\ &\quad - \{\sum_{n=1}^{3} [a_n'(T_j)] (\overline{S_iG_j})_n\} E_{g,j} \\ &\equiv \overrightarrow{S_iG_j} E_{s,i} - \overleftarrow{S_iG_j} E_{g,j} \end{aligned} \tag{4}$$

where $\overrightarrow{S_iG_j}$ and $\overleftarrow{S_iG_j}$ replace the terms in the brackets. These are called *directed-flux areas* since they are now dependent on the temperature of the emitting zone. (The tail of the arrow is placed above the letter designating the emitter.) In the above formulation allowance has been made for the configurations of the zones, for multiple reflection at the walls, for non-grayness of the gas, and for the temperature dependence of emissivity and absorptivity. It is the combination of these complicating factors which necessitate the development of the involved nomenclature given above.

(f) *Total energy balances*

Total energy balances are next formulated on the refractory surface zones and the gas zones. A balance on $A_i$ gives

$$\begin{aligned} \sum_j \overrightarrow{S_jS_i} E_{s,j} + \sum_j \overrightarrow{G_jS_i} E_{g,j} - A_i \epsilon_i E_{s,i} \\ + hA_i(T_{g,i} - T_{s,i}) = 0 \end{aligned} \tag{5}$$

where $T_{g,i}$ is the temperature of the gas zone contiguous to $A_i$. Similarly, a balance on a gas zone $V_i$ gives

$$\sum_j \overrightarrow{S_j G_i E_{s,j}} + \sum_j \overrightarrow{G_j G_i E_{g,j}} - 4\sum_n [a_n'(T_g)]\, K_n V_i E_{g,i} + \begin{pmatrix}\text{net enthalpy flux}\\ \text{into } i \text{ across its}\\ \text{boundaries}\end{pmatrix} + \begin{pmatrix}\text{net convective heat transfer}\\ \text{from contiguous surface}\\ \text{zones, if any}\end{pmatrix} + \begin{pmatrix}\text{combustion}\\ \text{in zone } i\end{pmatrix} = 0 \qquad (6)$$

The enthalpy fluxes are calculated from the mass flow rates across the boundaries and the specific enthalpies of gas evaluated at the temperature of the zone from which the gas flows. The eddy fluctuations are treated as two-way fluxes across the zone boundaries. Thirty simultaneous non-linear equations, six similar to (5) and twenty-four to (6), result. These can be solved by iterative techniques. A combination of the Gauss–Siedel and Newton–Raphson methods has been found to give rapid convergence to the exact solution. For example, in the balance on zone $i$, the temperatures of all zones but $i$ are guessed; the resulting non-linear equation in $T_i$ is solved by the Newton–Raphson method; the procedure is then repeated on the next zone after correction of the directed-flux areas associated with zone $i$ as an emitter. When successive iteratives on all zones agree within specified limits, convergence on the true solution is assumed.

(g) *Wall heat flux distribution*

Once the temperature distributions in the gas and along the refractory walls have been determined the net flux $\dot{Q}$ to the circumferential wall sink is calculated. Thus, at surface $i$,

$$\dot{Q}_{\text{net},i} = \sum_j \overrightarrow{G_j S_i E_{g,j}} + \sum_{j,\text{incl. } i} \overrightarrow{S_j S_i E_{s,j}} - A_i \epsilon_i E_i + hA_i(T_{g,k} - T_{s,i}) \qquad (7)$$

where $T_{g,k}$ is the temperature of the gas in zone $k$ contiguous to $A_i$. A check on the convergence of the solution given in (f) is provided by comparison of the sum of fluxes to the wall sinks with the decrease in total enthalpy of the gas flowing through the furnace.

By the above procedure a complicated integro-differential equation is replaced by a series of algebraic equations. The method is particularly well adapted to solution by high-speed digital computers. Further, some of the time-consuming steps are non-repetitive. Thus, the direct-exchange areas need be evaluated only once for a particular configuration; they are now available for systems expressible in Cartesian [11] and cylindrical [7] coordinates. Also, for a given furnace fired by a fixed fuel–air mixture, the effect of size and shape of the system, gas composition, and wall reflectances are handled once and for all in steps (c) and (d); studies of the effects of changes in flow rate or flow pattern, feed stream preheat, and temperature distribution of the controlled part of the wall can all be made by repeating steps (e) through (g) only.

## RESULTS

*Furnace efficiencies*

Table 3 presents the radiative heat flux, the convective heat flux, and the furnace efficiency for the range of conditions listed in Table 1. The unrealistically high recirculation ratio for a $Ct$ of 0·033 is responsible for the unusually high convective heat transfer in some of the runs. Discussion of these values is best withheld to a later section.

*Gas temperature distributions*

The effect of flow pattern on the gas temperature field is illustrated by the results on the 4-ft diameter furnace for a nominal firing density of $10^4$ Btu/h ft$^2$ of sink area. The profiles in Fig. 3 were obtained by interpolation between the 24 gas-zone temperatures; consequently, the regions with steep gradients are not well defined. As expected, the gas temperature falls off more rapidly near the wall than in the core for plug flow, and a similar but more pronounced trend is observed for the case of a parabolic velocity

*Table 3. Computed heat-transfer rates and efficiencies in cylindrical furnaces*

| Furnace dia. (ft) | Firing rate Btu/h per ft² of sink | Flow pattern (No. indicates Craya–Curtet number) | Convective ht. trans. Btu/h per ft² of sink | Radiative ht. trans. Btu/h per ft² of sink | Eff. (%) |
|---|---|---|---|---|---|
| 1 | $10^4$ | plug | 1253 | 5990 | 73·5 |
| 1 | $10^4$ | parabolic | 937 | 5780 | 68·5 |
| 1 | $10^4$ | 0·51 | 387 | 3615 | 40·8 |
| 1 | $4 \times 10^4$ | plug | 2865 | 15640 | 47·0 |
| 1 | $4 \times 10^4$ | parabolic | 2196 | 14080 | 41·0 |
| 1 | $4 \times 10^4$ | 0·51 | 670 | 6350 | 17·8 |
| 1 | $16 \times 10^4$ | plug | 10870 | 20640 | 20·0 |
| 1 | $16 \times 10^4$ | parabolic | 9570 | 19570 | 18·5 |
| 1 | $16 \times 10^4$ | 0·51 | 1278 | 8220 | 6·04 |
| 4 | $10^4$ | plug | 925 | 6450 | 74·9 |
| 4 | $10^4$* | parabolic | 791 | 6450 | 72·0 |
| 4 | $10^4$ | 0·51 | 442 | 4620 | 51·4 |
| 4 | $10^4$ | 0·18 | 689 | 5010 | 57·7 |
| 4 | $10^4$ | 0·033 | 1777 | 6090 | 63·6 |
| 4 | $4 \times 10^4$ | plug | 2270 | 20800 | 58·4 |
| 4 | $4 \times 10^4$ | parabolic | 1815 | 19230 | 53·1 |
| 4 | $4 \times 10^4$ | 0·51 | 705 | 9840 | 26·7 |
| 4 | $4 \times 10^4$ | 0·18 | 1933 | 13720 | 39·5 |
| 4 | $4 \times 10^4$ | 0·033 | 9630 | 11100 | 52·5 |
| 4 | $16 \times 10^4$ | plug | 7460 | 40400 | 30·3 |
| 4 | $16 \times 10^4$ | parabolic | 6450 | 36800 | 27·6 |
| 4 | $16 \times 10^4$ | 0·51 | 903 | 14900 | 9·97 |
| 4 | $16 \times 10^4$ | 0·18 | 9480 | 25200 | 22·0 |
| 4 | $16 \times 10^4$ | 0·033 | 43600 | 22060 | 41·5 |
| 16 | $10^4$ | plug | 709 | 6890 | 76·5 |
| 16 | $10^4$ | parabolic | 635 | 6750 | 75·0 |
| 16 | $10^4$ | 0·51 | 458 | 5310 | 58·1 |
| 16 | $4 \times 10^4$ | plug | 1750 | 24330 | 66·1 |
| 16 | $4 \times 10^4$ | parabolic | 1506 | 22950 | 62·0 |
| 16 | $4 \times 10^4$ | 0·51 | 756 | 15650 | 35·6 |

* Firing rate 2·1 per cent higher than the other runs.

profile. The effects of progress of combustion and rate of recirculation on the gas temperature profiles are very evident in the three diagrams for the ducted jet. A Craya–Curtet number of 0·51 corresponds to a slow-burning flame with little recirculation. For the particular flow rate shown, the temperature along the axis rises throughout the first 40 per cent of travel, where the increase in sensible enthalpy of the gas due to combustion more then compensates for the convective and radiative losses. The temperature gradients in the radial direction are largest in the transition region between the flame and the surrounding gases. The smaller values of *Ct* correspond to high rates of entrainment of surrounding fluid by the jet and hence higher combustion and recirculation rates. As a consequence of the increase in the combustion rate the maximum in the temperature along the axis is displaced towards the burner; and as a consequence of the increase in recirculation the temperature differences between the different zones in the furnace are reduced. Both of these effects are evident from a comparison of the runs for *Ct*'s of 0·51, 0·18 and 0·033.

*Wall heat-flux distribution*

The effect of flow patterns on the heat-flux distribution is illustrated by the results on the 4-ft diameter furnace for a firing density of $4 \times 10^4$ Btu/h ft² of sink area (see Fig. 4). For the plug flow and parabolic velocity profile

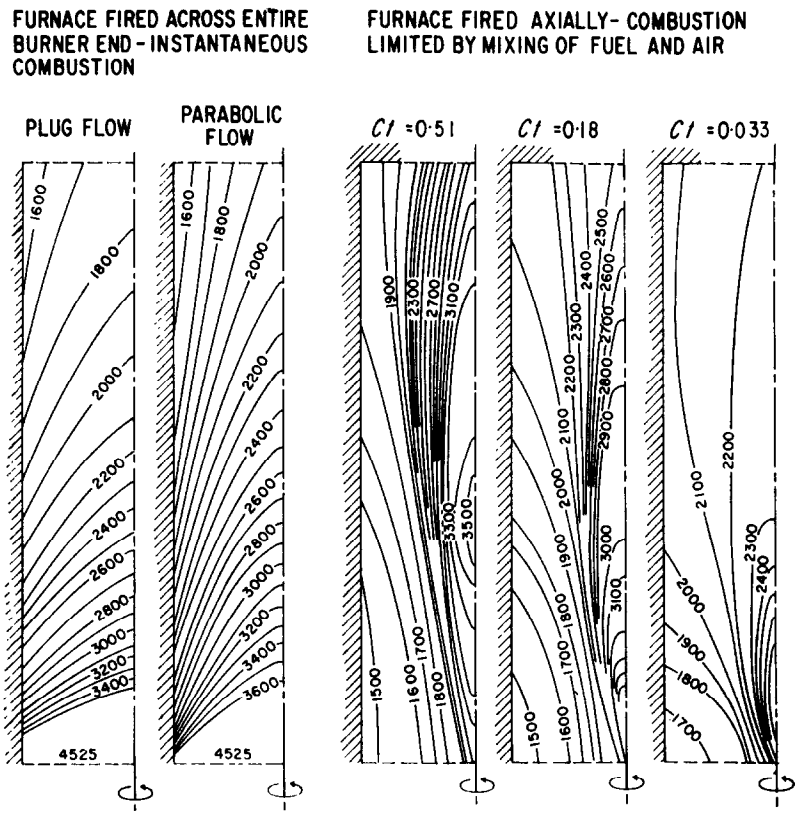


FIG. 3. Temperature profiles (in degrees Rankine) for a cylindrical furnace; diameter = 4 ft, firing density = $10^4$ Btu/h ft$^2$ of sink. Because of symmetry, the distribution to the left of the axis only is shown.

models the flux is a maximum near the burner end where the effective radiating temperature is a maximum; the wall flux falls off continuously along the length of the furnace as the gas temperature decreases. It is interesting to note that for the case shown the effective radiating temperature at the end of the furnace is higher for plug flow than for parabolic flow despite the fact that the higher efficiency of the plug flow model indicates that the mixed-gas leaving temperature for the plug flow model is smaller; the larger radial temperature gradients in the parabolic flow model are responsible for this apparent anomaly, which disappears at lower firing rates or for longer furnaces. For the ducted jets, the flux is a minimum at the burner end because the hot radiating gases occupy only a small volume in the center of the furnace. As the flame spreads the flux increases, but it must eventually pass through a maximum and fall off as the combustion products fill the entire cross section and as their temperature decreases. This expected decrease in wall flux is observed for the last surface zone at the lowest firing density (see Fig. 5). Increases in recirculation for ducted jets—corresponding to decreases in *Ct*—cause the heat flux distribution to even out (Fig. 4). Results for different firing densities and for other furnace diameters all showed a pronounced effect of flow patterns on heat flux distributions similar to that shown in Fig. 4.

## CORRELATION OF FURNACE PERFORMANCE

The results on furnace efficiencies were generalized by using a method of correlation originally proposed for well-stirred furnaces

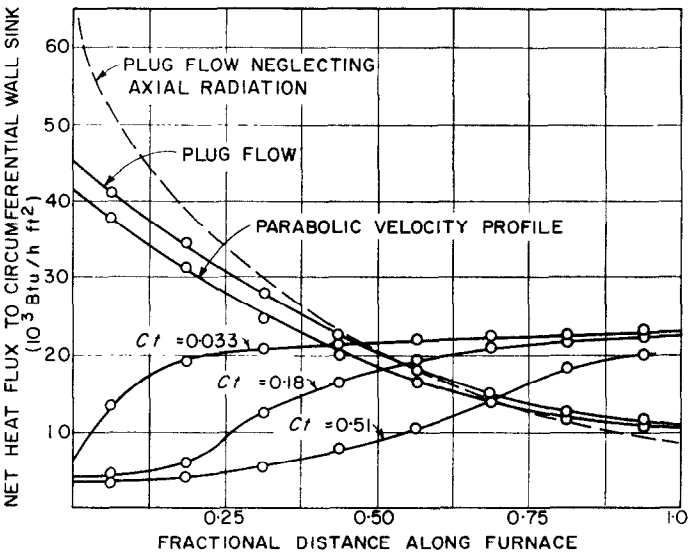


FIG. 4. Wall-flux distribution along cylindrical furnace calculated for different flow models; length-to-diameter ratio = 8/3, diameter = 4 ft, firing rate = $4 \times 10^4$ Btu/h ft² of sink.

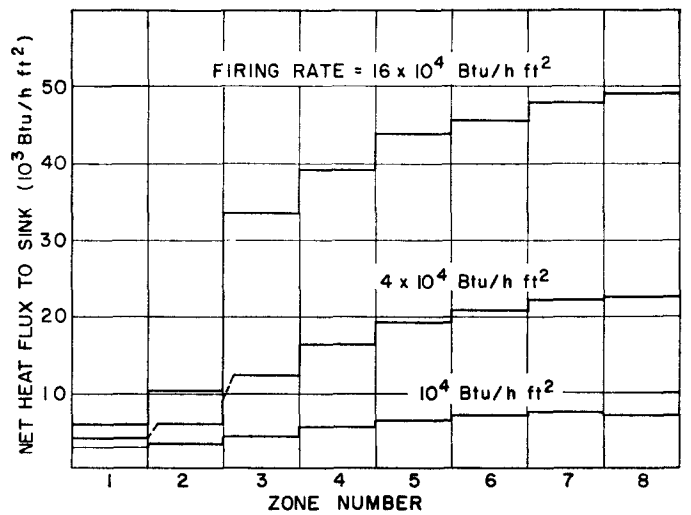


FIG. 5. Effect of firing density on heat-flux distribution; furnace diameter = 4 ft, $Ct = 0{\cdot}18$.

[12] and later extended to other flow models [13]. For a well-stirred gas in an enclosure containing a single isothermal sink, the gas-to-sink transport equation is

$$\dot{Q}_{g\rightleftharpoons s} = \overrightarrow{(GS)}_R \sigma T_g^4 - \overrightarrow{(SG)}_R \sigma T_w^4 + hA_S(T_g - T_w) \quad (7)$$

and the energy balance on the gas is

$$\dot{Q}_{g\rightleftharpoons s} = \dot{H}_{\text{in}} - \dot{M}C_p T_g \quad (8)$$

The enthalpies of the entering gases, $\dot{H}_{\text{in}}$, and the leaving combustion products, $\dot{M}C_pT_g$, are here evaluated above a base of $CO_2$, $H_2O$ (vapor), $O_2$, $N_2$ each equal to zero at absolute

zero. $\dot{M}C_p$ is the average hourly heat capacity over the temperature range 0 to $T_g$. The subscript $R$ on the directed-flux area is to indicate that allowance has been made for the assistance of the refractory in the transfer of radiation between gas and sink (see Appendix C). When the radiation from the gas is primarily due to emission by $CO_2$ and $H_2O$ it has been found [19] that, approximately,

$$\overrightarrow{GS}\,T_g = \overrightarrow{SG}\,T_w \tag{9}$$

A combination of (9) and (7) and linearization of the convection term in $T^4$ yields

$$\dot{Q}_{g\rightleftharpoons s} = \left\{(\overrightarrow{GS})_R\left[\frac{1-(T_w/T_g)^3}{1-(T_w/T_g)^4}\right] + \frac{h_c A_w}{\sigma T_{gw}^3}\right\} \sigma(T_g^4 - T_w^4) \tag{10}$$

where $T_{gw}$ is the average of the gas and sink temperatures. Elimination of $T_g$ between (8) and (10) and rearrangement gives the following relation

$$D' = \frac{(1-\dot{Q}_r)^4 - \tau^4}{\dot{Q}_r} \tag{11}$$

wherein

$$\dot{Q}_r \equiv \frac{\dot{Q}_{g\rightleftharpoons s}}{\dot{H}_{\text{in}}} \tag{12}$$

$$\tau \equiv T_w/T_{AF} \tag{13}$$

$$D' \equiv \frac{\dot{H}_{\text{in}}}{\left\{(\overrightarrow{GS})_R\left[\frac{1-(T_w/T_g)^3}{1-(T_w/T_g)^4}\right] + \frac{h_c A_w}{\sigma T_{gw}^3}\right\}\sigma T_{AF}^4} \tag{14}$$

$T_{AF} \equiv (H_{\text{in}}/\dot{M}C_p)$, with $\dot{M}C_p$ evaluated over the interval $T_g$ to 0. (15)

$D'$ may be considered to be a reduced firing density since it is the ratio of the enthalpy input to the furnace to a gas-to-surface heat-transfer rate based on a fictitious adiabatic flame temperature $T_{AF}$ given by equation (15); $\tau$ is a reduced sink wall temperature; and $\dot{Q}_r$ is a reduced efficiency differing from conventional efficiencies in that $\dot{H}_{\text{in}}$ is evaluated above a base temperature of absolute zero instead of 60°F. Equation (11) was used to calculate the line marked "well-stirred furnace" in Fig. 6, which also includes the results given in Table 3 and values calculated for a plug-flow model with no radial temperature gradients [19]. There are several interesting features of such a presentation of results:

(a) As the firing density $D'$ decreases the efficiency approaches $1 - \tau$. In this range the influence of $D'$ on efficiency is small. Physically this corresponds to conditions for which the exit gas temperature approaches the sink temperature.

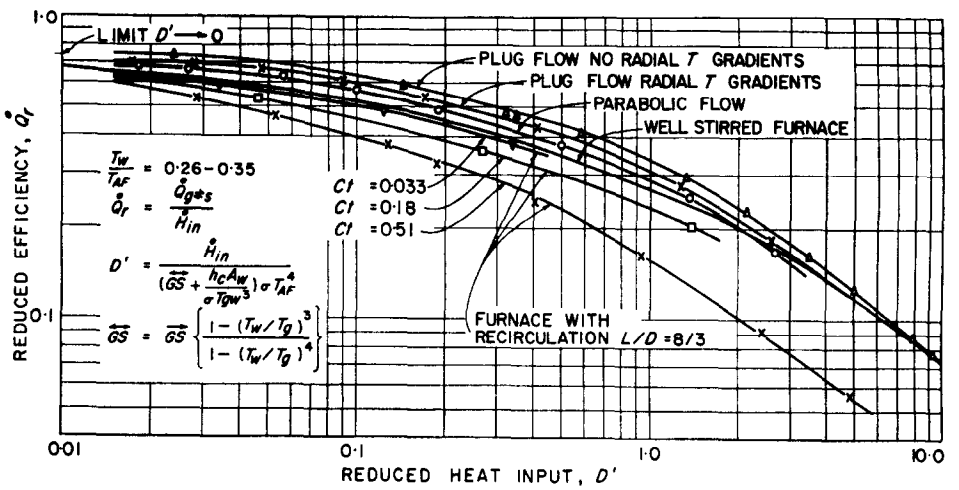


FIG. 6. Correlation of furnace efficiencies calculated for different flow models. Reduced heat input $D'$ is called reduced firing density in the text.

(b) Changes in sink temperature have relatively little influence on the furnace efficiency if the sink temperature is below 0·3 $T_{AF}$ [13].

(c) At extremely high firing rates the reduced efficiency becomes inversely proportional to $D'$. This corresponds to firing rates for which the temperature throughout the furnace approaches the adiabatic flame temperature (power-plant combustion chambers rather than furnaces).

The utility of this method of correlation is demonstrated by Fig. 6 which shows that the reduced efficiency for a range of furnace diameters of 1 to 16 ft can be correlated by a single line for each flow model. The plug flow and parabolic velocity profile models predict reduced efficiencies higher than those calculated for the well-stirred furnace.

The reduced efficiencies at $Ct = 0{\cdot}51$ are considerably lower than those for the well-stirred model. This is due to the reduction in flux caused by the small flame width near the burner and the slow progress of combustion along the furnace. As $Ct$ decreases the combustion and gas recirculation rates increase, and the reduced efficiency increases. The limit of infinite recirculation ($Ct \rightarrow 0$) is of course identical to the well-stirred model.

The utility of the above correlations is increased by the results obtained by Takeuchi [19] who showed that radiation from the gas along the axis of long furnaces is relatively small. Long furnaces can therefore be subdivided into different flow regions and the efficiency of each section obtained separately, starting at the burner end where $\dot{H}_{in}$ is known and working along the furnace. An approximation is introduced in that the enthalpy distribution of the gases entering a section will not match the distribution used in the calculations leading to the correlation in Fig. 6.

## LIMITATION OF RESULTS

The largest uncertainties in the results are due to the use of a finite number of zones in the calculations and the assumption of a uniform concentration throughout the enclosure.

The corrections applied to the direct-exchange areas to allow for temperature gradients within a gas zone were based on the assumption that $E$ varied linearly between the centers of the different zones*. Examination of the smoothed temperature profiles in Fig. 3 indicates that a finer zoning would be desirable about the edges of the flame for the calculations of the ducted jet, especially for a $Ct$ of 0·51.

Allowance is made for variation in gas emissive power due to variations in its temperature but not its concentration. The results for a $Ct$ of 0·51 will be the only ones significantly affected by this approximation since the circulation ratio for the other runs is sufficient to even out the concentration throughout most of the furnace. For a $Ct$ of 0·51, as a consequence of the assumption of a uniform concentration, the calculated radiative flux from the flame is falsely attenuated in passing through parts of the furnace which would normally be occupied by air. Consequently, the calculated fluxes to the first six wall sections are somewhat too small.

The above sources of error may be partially eliminated by use of a larger number of zones and an evaluation of exchange areas which allows for variation in concentration. Such modifications would greatly increase computation time, and need be considered only when the recirculation ratio is small. Since the computation of the results presented here took approximately 5 min of IBM 709 time per run, the increased computation time that would be associated with the inclusion of the above refinements would still be within the capabilities of available computers. A program which could allow for concentration gradients could be used also to evaluate the important effect of flame luminosity on the radiative transfer in furnaces.

## COMPARISON WITH FURNACE PRACTICE

Despite the above listed shortcomings of the method described here, it is based on a model which is clearly closer to reality than those used

* An alternative to the procedure of calculating exchange areas between isothermal zones and then applying a correction factor to allow for departure from temperature uniformity is the evaluation of exchange areas for a linear variation of $E$ between zone centers. This procedure has been used in radiative transfer calculations in unidimensional [18, 21] and two-dimensional temperature fields [5, 6].

in the past for prediction of furnace performance. No known prior models are capable of predicting the changed distribution of heat flux that is associated with burner design changes, i.e. with changing the entering fuel or air momentum without changing their mass flow; nor has any prior furnace model predicted the effect of changes in burner design on the gas temperature field in the furnace.

The testing of the validity of the detailed knowledge of furnace performance yielded by computations of the present type calls for a degree of sophistication and completeness of full-scale furnace testing almost never achieved in practice. Some experimental results of Litterscheidt [16] do, however, show the same trends as found here. He measured the local heat input along the walls of an end-fired cylindrical water-cooled furnace burning gaseous fuel in burners of different design.

When the fuel gas and air were premixed and combustion was completed in a small volume near the burner end, the rate of heat input to the wall showed a continuous decrease from 12 500 Btu/h ft$^2$ near the burner to 3700 Btu/h ft$^2$ at 8/3 diameters downstream. The trend is very similar to those shown in the present calculations by the plug-flow and parabolic-profile flow models.

When the fuel gas and air issued separately from a burner consisting of two concentric pipes at flow rates corresponding to a Craya–Curtet number of 0·26, the rate of heat input to the walls increased from a value of 2200 Btu/h ft$^2$ near the burner to a maximum of 5900 at 1·7 diameters downstream and then decreased to 5500 at an $L/D$ of 8/3. (Relative values 1, 2·7, 2·5). The heat flux for this case showed a distribution pattern similar to that found in the present calculations for $Ct = 0{\cdot}18$ and a firing rate of $10^4$ Btu/h ft$^2$ (Fig. 5; relative values 1, 2·7, 2·6).

Unfortunately, a quantitative comparison of the profiles is not possible since Litterscheidt's experimental conditions (Firing density = 14 800 Btu/h ft$^2$ of sink; adiabatic flame temperature, $T_{AF} = 3940°\text{R}$; $p_{H_2O} = 0{\cdot}208$ atm; $p_{CO_2} = 0{\cdot}065$ atm; "reduced" sink temperature, $T/T_{AF} = 0{\cdot}21$ to 0·28) differed from those used in the present calculations. However, it is possible to compare the generalized correlation of furnace efficiencies, Fig. 6, with Litterscheidt's results. The experimental conditions in his tests corresponded to a reduced firing density or heat input of 0·17; his measured heat fluxes corresponded to $\dot{Q}_r = 0{\cdot}60$ when the fuel and air were premixed and to $\dot{Q}_r = 0{\cdot}35$ when a double concentric pipe burner was used. From Fig. 6, it can be seen that $\dot{Q}_r = 0{\cdot}60$ lies somewhat above the lines calculated for plug- and parabolic-flow models and that $\dot{Q}_r = 0{\cdot}35$ is slightly below the value expected for a Craya–Curtet number equal to 0·26. Considering the differences in operating conditions, the predicted range of efficiencies produced by the variation in flow-pattern is in remarkably good agreement with the measured values; past methods of calculation would not have distinguished among the various flow types.

It is hoped that the ability to predict a reasonable amount of detail as to furnace performance will encourage the planning of full-scale furnace experiments to test the validity of the method. Progress in that direction is certain to indicate how the model presented here may be improved, and where simplifications are justified.

## CONCLUSIONS

Generalized flow and mixing patterns in cylindrical ducts have been used to calculate in a nearly rigorous manner the performance of cylindrical furnaces with a length-to-diameter ratio of 8/3. The results obtained for flow patterns corresponding to those of a ducted turbulent jet show that the assumption of simplified flow models such as plug flow may give very misleading results for the gas temperature and wall flux distributions. The strong dependence of wall flux distribution on flow patterns confirms what furnace designers already know—that flux patterns may be regulated by varying either burner arrangements or the momentum of the fuel jets.

"Reduced" efficiencies of furnaces over a very wide range of operation and design variables can be described in terms of a "reduced" firing density and the flow and combustion patterns only; correlations were obtained for each of five different flow models studied.

ACKNOWLEDGEMENT

The authors are grateful to the M.I.T. Computation Center for time provided on an IBM 709.

REFERENCES

1. H. A. BECKER, H. C. HOTTEL and G. C. WILLIAMS, *Ninth Symposium (International) on Combustion*, pp. 7–20. Academic Press, New York (1963).
2. H. A. BECKER, Sc.D. Thesis in Chemical Engineering, M.I.T. (1961).
3. J. M. BEÉR, N. A. CHIGIER and K. B. LEE, *Ninth Symposium (International) on Combustion*, Academic Press, New York (1963).
4. A. CRAYA and R. CURTET, *C.R. Acad. Sci., Paris* **241**, 621 (1955).
5. T. H. EINSTEIN, NASA Tech. Rept., R-154 (1963).
6. T. H. EINSTEIN, NASA Tech. Rept., R-156 (1963).
7. H. ERKKU, Sc.D. Thesis in Chem. Eng., M.I.T. (1959).
8. S. J. FRIEDMAN and A. C. MUELLER, *Proceedings General Discussion on Heat Transfer*, pp. 138–142. Instn Mech. Engrs, London, and Amer. Soc. Mech. Engrs, New York (1951).
9. W. R. HAWTHORNE, D. S. WEDDELL and H. C. HOTTEL, *Third Symposium on Combustion and Flame Explosion Phenomena*, p. 249. Williams and Wilkins, Baltimore (1949).
10. H. C. HOTTEL, Chapter 4 in W. H. MCADAMS, *Heat Transmission*, 3rd Ed. McGraw-Hill, New York (1954).
11. H. C. HOTTEL and E. S. COHEN, *J. Amer. Inst. Chem. Engrs* **4**, 3 (1958).
12. H. C. HOTTEL, *Notes on Furnaces and Furnace Measurements* M.I.T. (1957).
13. H. C. HOTTEL, *J. Inst. Fuel* **34**, 220 (1961).
14. H. C. HOTTEL and A. F. SAROFIM, Gaseous radiation with temperature gradients, allowance for isotropic scatter, *Theory and Fundamental Research in Heat Transfer* (Ed. J. A. CLARK), pp. 139–160. Pergamon Press, New York (1963).
15. H. C. HOTTEL, Some recent problems in radiative transport, in *International Development in Heat Transfer, Proceedings of the Heat Transfer Conference 1961–62*. Amer. Soc. Mech. Engrs, and Instn Mech. Engrs, London (1963).
16. W. LITTERSCHEIDT, *Gaswärme*, **3**, 84 (1955).
17. S. ROSSELAND, *Astrophysik und Atom-Theoretisches Grundlage*, p. 41. Springer Verlag, Berlin (1931).
18. A. F. SAROFIM, Sc.D. thesis in Chem. Engng, M.I.T. (1962).
19. S. TAKEUCHI, S. M. thesis in Chem. Engng, M.I.T. (1961).
20. R. VISKANTA and R. J. GROSH, *Appl. Mech. Rev.* **17**, 91 (1964).
21. V. A. WALTHER, J. DÖRR and E. ELLER, *Glastechn. Ber.* **26**, 133 (1953).

## APPENDIX A

*The Craya–Curtet number*

Define the kinematic-mean velocity $u_k$ as the average velocity of the gases entering the furnace. In terms of the mass fluxes $\dot{m}_N$ and $\dot{m}_I$ of the nozzle and induced streams, the gas density $\rho$ and the furnace cross sectional area $A_T$,

$$u_k = \frac{\dot{m}_N + \dot{m}_I}{\rho A_T} \tag{A-1}$$

Let the rates of momentum of the jet or nozzle stream and the induced stream be $i_N$ and $i_I$. Define the dynamic-mean velocity $u_d$ as that uniform entering velocity which produces a force equal to the excess of the true stream thrust $i_N + i_I$ over the stagnation pressure-area force of the induced stream $i_N/2$. Then

$$i_N + i_I - i_I/2 \equiv u_d^2 \rho A_T,$$

or

$$u_d^2 = \frac{i_N + i_I/2}{\rho A_T} \tag{A-2}$$

The Craya–Curtet number is defined by

$$Ct = \frac{u_k}{(u_d^2 - u_k^2/2)^{\frac{1}{2}}} \tag{A-3}$$

From the above definitions, it may be shown that for the case of a uniform stream velocity and a nozzle area negligible compared to the furnace cross section

$$Ct = \frac{1 + \dot{m}_I/\dot{m}_N}{\left[\left(\frac{\dot{m}_I}{\dot{m}_N}\right)^2 \frac{i_N}{i_I} - \frac{\dot{m}_I}{\dot{m}_N} - \frac{1}{2}\right]^{\frac{1}{2}}} \tag{A-4}$$

i.e. the flow is characterized by the ratios of the mass and momentum fluxes of the jet and induced streams.

## APPENDIX B

*Description of emissivities and absorptivities*

The $a$-weighting factors for use in equations (2) and (3) were described by third-order polynomials of the form

$$a_n = a_{n0} + a_{n1}T + a_{n2}T^2 + a_{n3}T^3$$

The values of the coefficients are given in Table B-1. The values used in the calculations on the 1 ft and 4 ft diameter furnaces describe emissivities and absorptivities for path-lengths of 0·02 to 15 ft; the values used for the 16 ft diameter

*Table* B-1. *Polynomials defining gas emissivity and absorptivity*

| | $n$ | $K_n$(ft$^{-1}$) | $a_{n0}$ | $a_{n1} \times 10^4$ | $a_{n2} \times 10^7$ | $a_{n3} \times 10^{11}$ |
|---|---|---|---|---|---|---|
| $\epsilon_g$(0·02–15 ft) | 1 | 0·1288 | 0·3029 | 0·9120 | −0·4930 | 0·5000 |
| $\epsilon_g$(0·02–15 ft) | 2 | 1·334 | 0·1043 | 0·2946 | −0·2658 | 0·3560 |
| $\epsilon_g$(0·02–15 ft) | 3 | 11·62 | 0·1857 | −1·293 | 0·3364 | −0·3110 |
| $\alpha_g$(0·02–15 ft) | 1 | 0·1288 | 0·4176 | 1·082 | −0·9771 | 1·443 |
| $\alpha_g$(0·02–15 ft) | 2 | 1·334 | 0·1390 | 0·2320 | −0·3462 | 0·5555 |
| $\alpha_g$(0·02–15 ft) | 3 | 11·62 | 0·0486 | 0·1677 | −0·2034 | 0·350 |
| $\epsilon_g$(0·2–45 ft) | 1 | 0·04439 | 0·7961 | 3·544 | −1·273 | 1·229 |
| $\epsilon_g$(0·2–45 ft) | 2 | 0·5159 | 0·3571 | −1·385 | 0·2367 | −0·1796 |
| $\epsilon_g$(0·2–45 ft) | 3 | 6·118 | 0·1250 | −0·3402 | −0·0159 | 0·0761 |
| $\alpha_g$(0·2–45 ft) | 1 | 0·04439 | 0·3216 | 4·397 | −2·705 | 4·050 |
| $\alpha_g$(0·2–45 ft) | 2 | 0·5159 | 0·2617 | −0·01360 | −0·3760 | 0·7000 |
| $\alpha_g$(0·2–45 ft) | 3 | 6·118 | −0·6598 | 2·256 | −1·168 | 1·740 |

furnace are valid over a range of 0·2 to 45 ft. The emissivities were evaluated over a temperature range of 2000 to 4000°R; and the absorptivities were evaluated for an average gas temperature of 2500°R and a surface temperature range of 1000° to 3000°R.

## APPENDIX C

*Derivation of* $(\overrightarrow{GS_W})_R$ and $(\overleftarrow{GS_W})_R$

Let the furnace enclosure consist of a single well-stirred gas zone, a sink $A_W$ covering the circumferential wall, and an adiabatic refractory surface $A_e$ covering both end walls. It is desired to calculate directed-flux areas $(\overrightarrow{GS_W})_R$ and $(\overleftarrow{GS_W})_R$ between gas and sink which include the assistance provided by the refractory in transferring radiation between the two, such that

$$(Q_{g \rightleftharpoons W})_{R,\,\text{radiation}} \equiv (\overrightarrow{GS_W})_R E_g - (\overleftarrow{GS_W})_R E_W \tag{C-1}$$

First the total-exchange areas between all zone pairs are evaluated, with the refractory treated as a source-sink. An energy balance on the refractory gives

$$\overrightarrow{GS_e}E_g + \overrightarrow{S_WS_e}E_W + \overrightarrow{S_eS_e}E_e + h_eA_e(T_g - T_e) = A_e\epsilon_eE_e \tag{C-2}$$

Equation (C-2) may be solved for $E_e$ after replacing $h_eA_eT_e$ by $(h_eA_e/\sigma T_e^3)E_e$. The value of $E_e$ thus obtained may be substituted into the transport equation,

$$(Q_{g \rightleftharpoons W})_{R,\,\text{radiation}} = \overrightarrow{GS_W}\,E_g + \overrightarrow{S_eS_W}\,E_e + \overrightarrow{S_WS_W}\,E_W - A_W\epsilon_W\,E_W \tag{C-3}$$

A comparison of the terms in the resulting equation with those in (C-1) yields

$$(\overrightarrow{GS_W})_R = \overrightarrow{GS_W} + \frac{\left(\overrightarrow{GS_e} + \dfrac{h_eA_e}{\sigma T_g^3}\right)\overleftarrow{S_WS_e}}{A_e\epsilon_e + \dfrac{h_eA_e}{\sigma T_e^3} - \overrightarrow{S_eS_e}} \tag{C-4}$$

and, after some additional manipulation,

$$(\overleftarrow{GS_W})_R = \overleftarrow{GS_W} + \frac{\left(\overrightarrow{S_eG} + \dfrac{h_eA_e}{\sigma T_e^3}\right)\overrightarrow{S_WS_e}}{A_e\epsilon_e + \dfrac{h_eA_e}{\sigma T_e^3} - \overrightarrow{S_eS_e}} \tag{C-5}$$

For the evaluation of $(\overrightarrow{GS_W})_R$ and $(\overleftarrow{GS_W})_R$, $T_e$ may be assigned a value equal to the average of $T_g$ and $T_W$. $(\overrightarrow{GS_W})_R$ and $(\overleftarrow{GS_W})_R$ are equivalent to $A_1\mathscr{F}_{1\leftarrow G}$ and $A_1\mathscr{F}_{1\rightarrow G}$ of [10].

*Table* D-1. *Convection coefficients to the circumferential and end surfaces*

| Furnace diameter (ft) | Firing rate ($10^4$ Btu/h ft$^2$ of sink) | Flow pattern (Numbers correspond to *Ct* values) | $h_e$ (Btu/h ft$^2$ °F) | $h_w$ (Btu/h ft$^2$ °F) |
|---|---|---|---|---|
| 1 | 1 | Plug, parab., 0·51 | 3·1 | 1·5 |
| 1 | 4 | Plug, parab., 0·51 | 6·6 | 1·5 |
| 1 | 16 | Plug, parabolic | 8·8 | 4·2 |
| 1 | 16 | 0·51 | 8·8 | 2·1 |
| 4 | 1 | Plug, parab., 0·51, 0·18 | 3·1 | 1·5 |
| 4 | 1 | 0·033 | 3·1 | 3·1 |
| 4 | 4 | Plug, parab., 0·51 | 6·6 | 1·5 |
| 4 | 4 | 0·18 | 6·6 | 1·9 |
| 4 | 4 | 0·033 | 6·6 | 9·0 |
| 4 | 16 | Plug, parabolic | 8·8 | 3·2 |
| 4 | 16 | 0·51 | 8·8 | 1·5 |
| 4 | 16 | 0·18 | 8·8 | 5·8 |
| 4 | 16 | 0·033 | 8·8 | 27·0 |
| 16 | 1 | Plug, parab., 0·51 | 3·1 | 1·5 |
| 16 | 4 | Plug, parabolic | 6·6 | 3·2 |
| 16 | 4 | 0·51 | 6·6 | 1·5 |

**Résumé**—La prévision des performances des fours industriels est estimée classiquement en faisant des hypothèses grossières sur l'effet des variations de température dans le gaz. La méthode des zones pour tenir compte de l'effet sur le transport par rayonnement, de la variation de température à l'intérieur des fours a été appliquée au problème de l'interaction entre le rayonnement et les autres modes de transport de chaleur. L'effet de configurations différentes d'écoulement sur le champ de température du gaz et la distribution de flux pariétal dans un four cylindrique a été examiné en utilisant les modèles d'écoulement suivants: écoulement en bloc; profils de vitesse paraboliques; écoulement de jet canalisé (alimentation axiale) avec des vitesses de recirculation de 0,1 et 11 fois la vitesse d'écoulement du gaz de carneau. Une gamme de diamètres et de densités de chauffe variant dans un rapport de 1 à 16 a été étudiée. Les rendements réduits ont été corrélés, pour une température de surface fixée et pour chacun des modèles d'écoulement, en fonction d'une vitesse réduite de chauffe. La gamme étendue des configurations de distributions de flux de chaleur trouvéée dans l'étude souligne la nécessité de tenir compte de la variation de la température du gaz dans une analyse quelconque de four dans laquelle la configuration de flux de chaleur est importante.

**Zusammenfassung**—Die Voraussage der Leistung von Industrieöfen wird gewöhnlich abgeschätzt, indem für den Einfluss der Temperaturänderungen im Gas grobe Annahmen getroffen werden. Um beim Wärmeübergang durch Strahlung den Einfluss der Temperaturänderungen im Ofenmantel mit in Betracht zu ziehen, wurde die "Zonenmethode" für das Problem der Wechselwirkung zwischen Strahlung und anderen Arten des Wärmeüberganges angewandt. Der Einfluss verschiedener Strömungsarten auf das Temperaturfeld des Gases und die Verteilung der Wärmestromdichte in der Wand in einem zylindrischen Ofen wurde unter Verwendung folgender Strömungsmodelle untersucht: Kolbenströmung; parabolische Geschwindigkeitsprofile; geführte Strahlströmung (axiale Zuleitung) mit Umwälzgeschwindigkeiten von 0,1, und 11 mal der Rauchgasstromgeschwindigkeit. Es wurde ein sechzehnfacher Bereich von Durchmessern und Brenndichten untersucht. In Termen einer reduzierten Brenngeschwindigkeit wurden die reduzierten Wirkungsgrade für eine feste Oberflächentemperatur und für jedes Strömungsmodell untereinander in Beziehung gesetzt. Der weite Bereich des Verteilungsmodells der Wärmestromdichten, das sich bei dieser Untersuchung ergab, betont die Notwendigkeit, die Änderung der Gastemperatur bei jeder Ofenanalyse, bei dem die Art des Wärmestromes wichtig ist, mit zu berücksichtigen.

**Аннотация**—Теоретический расчет работы промышленных печей обычно производится при наличии больших допущений относительно влияния изменений температуры газа. Зональный метод, учитывающий влияние изменений температуры стенок печи, был применен к проблеме взаимодействия между излучением и другими способами переноса

тепла. Влияние различных полей скорости на температурное поле газа и распределение тепловго потока через стенки в цилиндрической печи исследовались с помощью следующих моделей потока: равномерный профиль скорости, параболические профили скоростей; струйное течение в канале (аксиальная подача) при отношениях расхода рециркулирующих газов к расходу дымовых газов, равных 0,1 и 11. Изучались шестнадцатикратный диапазон диаметров и форсировок. Были подсчитаны приведенные к.п.д. для фиксированной температуры поверхности и для каждой из моделей течения в зависимости от форсировки. Обнаруженный при исследовании широкий диапазон распределений тепловых потоков подчеркивает необходимость учета изменения температуры газа при любом теоретическом анализе работы печей, в котором распределение тепловго потока является важным.